Al-Nahrain Journal for Engineering Sciences **NJES** 28(4)515-523, 2025
http://doi.org/10.29194/NJES.28040515

Antenna Design for Ultra-Wideband System Using a Fractal H-Shaped Structure for Enhanced Filtering and Narrowband Operation

Noor K. Mohsin [1], Dhirgham K. Naji [2*]

Authors affiliations:
1) Department of Electronics and Communications Engineering, Al-Nahrain University, Baghdad-Iraq.
eng.n99r@gmail.com

2*) Department of Electronics and Communications Engineering, Al-Nahrain University, Baghdad-Iraq.
dhrgham.kamal@gmail.com

Paper History:

Received: 8th Jan. 2025

Revised: 10th Mar. 2025

Accepted: 9th Apr. 2025

Abstract

In this work, for ultra-wideband (UWB) applications, a passive filter antenna with edge chamfering is investigated in this paper. The performance of an optimized UWB antenna design that achieves an advanced fractional impedance bandwidth of 102% is confirmed by simulation and experimentation. The performance of the antenna is improved by integrating a lowpass filter (LPF) into the fed line, which suppresses high-frequency radiation with a central frequency of 3.5 GHz (WiMAX), the UWB antenna has been transformed into a narrowband antenna, offering a 43.7% fractional bandwidth that spans the frequency range from 2.7 GHz to 3.9 GHz. A stepped impedance transmission line and an extended fractal H-shaped structure integrated in the microstrip feedline make up the filtering network. Using CST Microwave Studio (CST MWS), key performance parameters such as the radiation patterns, efficiency, gain, and reflection coefficient (S11) were examined. In its prototype, the antenna reduces its size by 5% and is made on a FR4 substrate with a permittivity coefficient of 4.3 and a loss tangent of 0.02. A maximum gain of 1.7 dBi and a peak efficiency of 78% at the center frequency were verified experimentally. The center frequency was verified experimentally. The tiny antenna, which measures $0.30\lambda_o \times 0.37\lambda_o \times 0.008\lambda_o$, performs well and is appropriate for UWB applications. The design makes a significant addition to the realm of UWB technology by incorporating elements that improve its ability to adapt.

Keywords: Low-Pass Filter, Passive Filtering, Ultra-Wideband.

تصميم هوائي ذو نطاق فائق العرض يتميز باستخدام شكل كسوري على شكل H بهدف تحسين قمع الترددات خارج النطاق

نور كريم محسن، ضرغام كمال ناجي

الخلاصة:

تتناول هذه البحث هوائيًا مفلترًا سلبيًا مزودًا بتشذيب للحواف للتطبيقات ذات النطاق الترددي عريض جدًا .(UWB) تم اقتراح تصميم هوائي UWB محسن يحقق عرض نطاق مقاومة كسري متقدم بنسبة ١٠٢٪، وتم التحقق من أدائه من خلال النتائج التجريبية والمحاكاة. يعمل دمج مرشح الترددات المنخفضة (LPF) في خط التغذية على تحسين أداء الهوائي من خلال قمع الإشعاع عالي التردد. يعمل هذا الابتكار على تحويل هوائي UWB إلى هوائي نطاق ضيق متمركز عند ٣,٥ جيجا هرتز (WiMAX) ، مع عرض نطاق بنسبة ٤٣,٧٪ يغطي الترددات من ٢,٧ جيجا هرتز إلى ٣,٩ جيجا هرتز .تتكون شبكة التصفية من خط نقل بممانعة متدرجة وهياكل ممتدة فراكتاليه على شكل حرف H المدمجة مع خط التغذيه المايكروسترب. تم تحليل مؤشرات الأداء الرئيسية، بما في ذلك معامل الانعكاس(S11) ، الكسب، الكفاءة، وأنماط الإشعاع باستخدام برنامج CST Microwave Studio (CST MWS). تم تصنيع الهوائي على ركيزة FR4 ذات سماحية نسبية ٤,٣ ومعامل فقد ٠,٠٢ ، وحقق تقليلًا في الحجم بنسبة ٥٪ في النموذج الأولي. أظهرت النتائج التجريبية تحقيق كفاءة قصوى بلغت ٧٨٪ وكسبًا أقصى يبلغ ١,٧ ديسي بل عند التردد المركزي. يظهر الهوائي المدمج، بأبعاد $0.008\lambda_o \times 0.37\lambda_o \times 0.30\lambda_o$ حيث λ_o هو الطول الموجي في الفضاء الحر عند الرنين، أداءً فعالًا وملاءمة للتطبيقات ذات النطاق الترددي العريض جدًا. يتضمن التصميم ميزات تعزز من مرونته، مما يجعله مساهمة قيمة في مجال تقنية.UWB.

1. Introduction

Modern wireless communication systems increasingly favor ultra-wideband (UWB) antennas due to their ability to deliver high data rates and wide bandwidth with minimal power consumption. However, a significant challenge associated with these antennas is out-of-band signal interference, which can adversely affect the system's overall performance [1]. A practical approach to addressing this issue in antenna design is to integrate filtering functionalities, offering improved compactness and enhanced electromagnetic performance [2]. Notably, integrating specific filtering topologies directly into the antenna feed allows for tuning of both radiation and rejection characteristics. The integration of feed lines with H-unit cells in UWB antennas reduces distortion within the passband of individual filters, ensuring high efficiency and compact equipment size. This method, detailed in [3], delivers these advantages while maintaining low system complexity. The proposed design offers a compact solution for UWB applications and demonstrates improved out-of-band rejection [4]. This study adds to the continuous development of multifunctional antenna technology for next-generation communication systems by combining theoretical analysis with experimental validation [5].

The literature extensively explores design methods for the radiating elements of filtering antennas, including the use of vias, stubs, slots, notches, and shorts [6–11]. These techniques not only enhance out-of-band rejection but also significantly reduce antenna size and operating bandwidth [12]. However, they often compromise filter selectivity by removing certain essential components. Open-loop filter resonators, electrically linked to the radiator, have been employed to isolate specific frequency bands, as demonstrated in [7, 8]. Although effective, this method introduces considerable structural complexity and results in a reduction in gain, primarily due to coupling inefficiencies.

Recent advancements have focused on integrating filters with radiating elements using two main approaches: (1) embedding a filter network within the feed line of the primary radiating structure, and (2) directly incorporating filtering elements into the antenna, utilizing additional components such as strips, switches, and biasing circuits. While these techniques are innovative, they face challenges in maintaining compact designs and often necessitate matching networks to ensure operation across multiple frequency bands [9]. For instance, a triangular ring stub-based multimode resonator, inter-digitally coupled with the microstrip feed line, has been used to suppress out-of-band signals in UWB monopole antennas, as discussed in [10]. Enhanced coupling was achieved by removing the ground plane beneath the coupling region.

Similarly, [12] describes a multi-mode resonator filter integrated with an elliptical patch monopole antenna, paired with a 50 Ω microstrip feed line, for cognitive radio applications. These developments offer promising solutions for addressing the challenges of filtering and multi-frequency operation in antenna systems. The antenna exhibits tunability between C-band and UWB frequencies using PIN diode switches, but its overall gain is limited due to the power distribution across the broad frequency range. In [13], a bowtie-shaped UWB antenna integrated with a fork-shaped resonator filter along the feed line is presented, providing tunability across UWB, 3.5 GHz, and 5.5 GHz by adjusting the diode switch states. Although the antenna demonstrates good radiation characteristics and gain, its large size and high structural complexity are significant drawbacks. A compact tunable filtering UWB antenna is proposed in [14], incorporating H- and T-shaped resonator filters integrated into the feed line. The design, fabricated on an RO3003™ substrate, uses a varactor and biasing circuit to achieve frequency band tunability.

Additionally, the inclusion of a defected ground structure improves insertion loss and enhances coupling efficiency between the feed line and the microstrip radiator. Similarly, [15] presents a compact tunable band-pass filtering UWB antenna with a symmetrical ring resonator coupled to the microstrip feed line. Built on a ROGERS3003 substrate, this antenna achieves a gain of over 1.5 dBi. However, its relatively low gain is attributed to losses from additional components. The varactor, supported by a biasing circuit, enables continuous frequency tuning within a narrow range, showcasing the antenna's frequency agility for advanced applications.

After refining each individual component, the researchers expanded their efforts to develop a multipurpose system that integrates both the filter and antenna into a single module. This innovative design enables simultaneous radiation and filtering capabilities, streamlining communication systems and leading to the creation of what is known as a "filtenna" or filtering antenna [16–20]. Various filtenna designs have been explored, including those combining patch antennas with hairpin filter technology. For instance, a new printed monopole antenna featuring a stepped impedance hairpin resonator (SIHR) was developed in [21] to operate at 2.53 GHz. This design, fabricated on the high-cost Rogers RO4003C substrate, achieved a gain of approximately 2.63 dBi. In contrast, a compact wideband filtenna utilizing a synthesis approach was proposed in [22], where the radiating element was integrated with the final-order resonator of a hairpin filter. Although this design used the more cost-effective FR4 substrate, it exhibited notable insertion losses of −2.5 dB.

In this study, a new compact filtering antenna with harmonic suppression and high selectivity is designed, inspired by the concept of integrating an H-shaped fractal low-pass filter (LPF) into the feedline of a UWB antenna. This design introduces a radiation null in the upper side of the gain response, providing enhanced out-of-band suppression. Key performance metrics, including the reflection coefficient (S_{11}), gain, efficiency, and radiation patterns, are analyzed using CST MWS. Prototypes of the H-shaped fractal filter, UWB antenna, and filtering antenna are fabricated, and the measured results are compared with the simulated results to verify the design's performance.

2. The UWB Antenna Design

In this paper, a new UWB antenna is presented,. This design has a UWB frequency band (from 2.7 GHz to 7.6 GHz). The structure is fabricated on a compact FR4 Epoxy substrate with a dielectric constant of $\varepsilon_r = 4.3$ and a loss tangent of tan(δ) = 0.020. Antenna simulations are conducted using Computer Simulation Technology (CST) Studio Suite, as shown in Fig. (1).

The UWB antenna previously discussed is considered to be integrated into a 3.5 GHz narrow-band radio. Due to the limited signal-to-noise (SNR) capability of the transceiver, noise was received. To address this, a feed line-integrated filter is incorporated into the transceiver design, complementing the built-in filter. By adding the feed line filter, filter overhead is reduced, and the overall out-of-band performance of the communication system is enhanced.

2.1 Design steps and principle of UWB antenna

The five design steps for evaluating the performance of the suggested UWB antenna are described in this section. Fig. (2) illustrates these design steps, with their geometric parameters listed in Table (1). The reflection coefficient (s_{11}) curves are shown in Fig. (3). The five designs are discussed, and their performance is described in detail as follows:

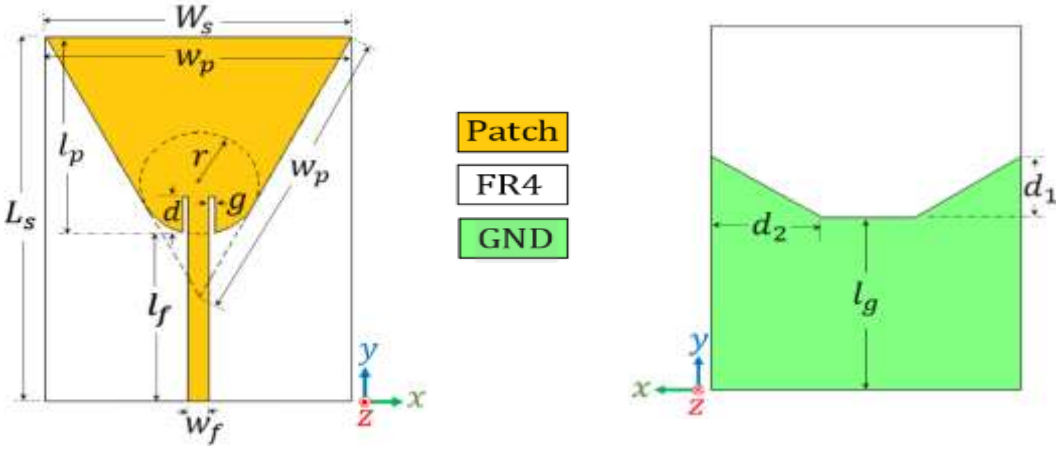

(a) (b)

Figure (1): Geometrical design of the UWB. (a) Front side . (b) Back side .

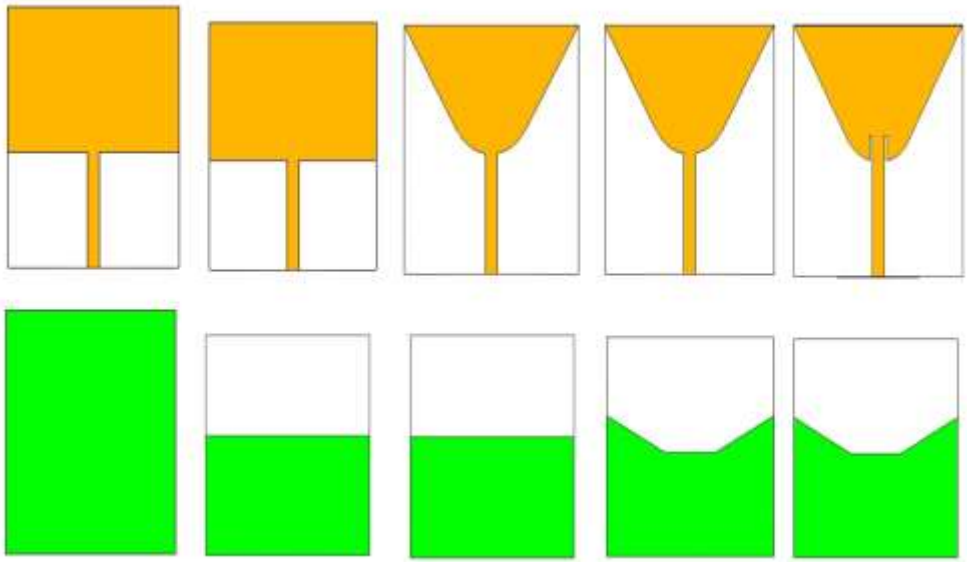

(a) (b) (c) (d) (e)

Figure (2): Design evolution of proposed antennas: **(a)** Ant.1. **(b)** Ant.2. **(c)** Ant.3. **(d)** Ant.4. **(e)** Ant.5.

Table (1): Dimension details of the proposed UWB antenna.

Parameter Name	Value (mm)
W_s	29
L_s	35
l_p	19
w_p	29
w_f	2
l_f	16
l_g	16.6
r	11
d_1	6
d_2	10
d	3.5

g	0.3
h_s	0.8

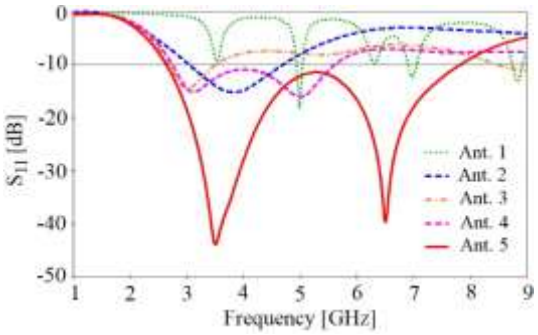

Figure (3): Reflection coefficient characteristics of the evolution steps of the UWB antenna.

Step I (Ant. 1): In this step, a conventional Rectangular Microstrip Antenna (RMSA), as shown in Fig. (2a), is designed based on transmission line model. The design is based on the following specifications: resonant frequency $f_r = 3.5\ \text{GHz}$, dielectric constant $\varepsilon_r = 4.3$ (FR4), and substrate height $h_s = 0.8\ \text{mm}$. The patch dimensions are obtained as $w_p = 29\ \text{mm}$ and $l_p = 22\ \text{mm}$. The total substrate dimensions are $L_s \times W_s = 36 \times 29\ \text{mm}^2$, with the patch width and length $w_p = Ws = 29\ \text{mm}$ and $L_s = 36\ \text{mm}$, respectively. As observed in Figure (3), Ant. 1 exhibits four resonant frequencies at 3.5 GHz, 4.9 GHz, 6.23 GHz, and 7.02 GHz, . By taking into account these values, the patch dimensions l_p and w_p for the dominant TM_{010} mode can be estimated by using Eqns. (1)-(4) [1]

$$l_p = \frac{v_0}{2f_r\sqrt{\varepsilon_{eff}}} - 2\Delta l_p \quad \ldots\ldots (1)$$

$$w_p = \frac{v_0}{2f_r\sqrt{(\varepsilon_r+1)/2}} \quad \ldots\ldots (2)$$

$$\Delta l_p = 0.412h_s\frac{(\varepsilon_{eff}+0.300)\big((w_p/h_s)+0.262\big)}{(\varepsilon_{eff}-0.258)\big((w_p/h_s)+0.813\big)} \ldots (3)$$

$$\varepsilon_{eff} = \frac{\varepsilon_r+1}{2} + \frac{\varepsilon_r-1}{2}\frac{1}{\sqrt{1+12(h_s/w_p)}} \quad \ldots\ldots (4)$$

where Δl_p ε_{eff}, and v_0 are extension of l_p due to the fringing field, the effective dielectric constant of the substrate, and velocity of light in free space, respectively.

By applying these equations, the geometrical parameters of the conventional RMPA have been calculated as $l_p = 20.52\ \text{mm}$ and $w_p = 26.32\ \text{mm}$. Then, the RMPA is simulated by employing the full wave electromagnetic CST MWS with the calculated values of l_p and w_p mentioned above as an initial dimensions. Then, on the front side of the substrate, a rectangular patch with dimension $w_p \times l_p$ is connected to the 50Ω SMA connector through the microstrip feedline of length $l_f = 16\ \text{mm}$ and width $w_f = 2\ \text{mm}$. A complete metallization ground plane is printed on the back side of the substrate. By fine-tuning the antennas' geometrical parameters via CST simulator for resonating at $f_r = 3.5\ \text{GHz}$, the optimized patch dimensions have obtained as $l_p = 19\ \text{mm}$ and $w_p = 29\ \text{mm}$. The total substrate dimensions ($W_s \times L_s$) of ($29 \times 35\ \text{mm}^2$) is used for the RMPA. Three resonance frequencies f_{r1}, f_{r2}, and f_{r3} of 3.51, 4.91, and $6.19\ \text{GHz}$ corresponding to TM_{010}, TM_{002}, and TM_{020} modes, respectively are excited by the antenna, as shown in Fig. 3(a). These three resonance frequencies can be calculated by [1]

$$(f_r)_{mnp} = \frac{v_0}{2\pi}\sqrt{\left(\frac{m\pi}{h_s}\right)^2 + \left(\frac{n\pi}{l_p}\right)^2 + \left(\frac{p\pi}{w_p}\right)^2} \quad \ldots (5)$$

Substituting in (5), $h_s = 0.8\ \text{mm}$, $l_p = 19\ \text{mm}$, and $w_p = 29\ \text{mm}$, gives the lowest three resonant frequencies (dominant modes), $(f_r)_{010}$, $(f_r)_{002}$, and $(f_r)_{020}$ as 3.8, 5.5, and 7.6 GHz, respectively. This reference antenna serves as the foundation for designing the proposed filtering antenna ,forming a narrow band, whereas the proposed antenna is designed to cover a wideband.

Step II (Ant. 2): In this step, Ant. 2 is designed by modifying the ground plane length using a partial ground technique, where $l_g = 16.6\ \text{mm}$, instead of the full ground length of $l_g = L_s = 36$ used in Antenna 1. This value of l_g is kept constant for all subsequent antennas (Ant. 2 through Ant. 5). As shown in Figure (3), Ant. 2 exhibits a matching bandwidth of greater than −10 dB, spanning from 3.1 GHz to 4.69 GHz for $s_{11} \leq -10\ \text{dB}$, with a resonance frequency of 3.8 GHz and a minimum reflection coefficient of −15.27 dB. Additionally, the antenna size is compact, with a reduction of approximately 5% compared to Step 1. The dimensions of the antenna are as follows: the width and length of the patch are $w_p = W_s = 29\ \text{mm}$, the total length is $L = Ls = l_p + l_f = 35\ \text{mm}$, and the patch length is $l_p = 19\ \text{mm}$.

Step III (Ant. 3): In this step, impedance matching is further optimized by chamfering the edges of the rectangular patch, resulting in a beveled monopole antenna, as illustrated in Fig. (1a). Chamfering is a well-established method for improving both the realized bandwidth and impedance matching of antennas. The impedance matching can be fine-tuned by adjusting the chamfering radius, referred to as r. This radius is varied incrementally to achieve optimal impedance matching across the UWB frequency range. The ideal radius of '$11\ \text{mm}$' is selected, and at this stage, a circular radius r is added at the end of the feed line, tangent to the chamfered edges, to achieve the desired resonance frequency. Enhanced impedance matching is observed in the frequency range of 2.7–3.5 GHz with a resonance frequency at 3 GHz, and reflection coefficient of −14.57, as shown in Fig. 3. Consequently, Antenna 3 serves as the reference, covering the lower-frequency Wi-Fi and upper-frequency WiMAX applications.

Step IV (Ant. 4): In this step, two triangles are added to the upper edge of the ground plane ($d_1 = 6\ \text{mm}$, $d_2 = 10\ \text{mm}$) to extend the bandwidth from a narrow to a wide range while maintaining the same resonance frequency of 3 GHz. This modification enhances the antenna's performance and shifts the band to cover the range from 2.7–5.64 GHz. The 3.5 GHz band, which considers high-frequency components as noise, is still

picked up by the UWB antenna. However, this results in a reflection coefficient of -16.43 . The antenna now covers both Wi-Fi and WiMAX frequency ranges.

Step V (Ant. 5): In the fifth and final step of the design procedure, an inset-fed structure is incorporated into the patch, designed according to specific parameters: length $d = 3.5$ mm and width $g = 0.3$ mm This inset-fed geometry is aligned with the chamfered edge of the antenna's radiating patch, which enhances the capacitive effect and facilitates improved impedance matching across a wide bandwidth. The configuration is shown in Figure (2) (Ant. 5). The proposed chamfered-edge UWB antenna, depicted in Fig. (1), achieves a fractional bandwidth of 102%, operating within the UWB frequency range of 2.54 to 7.46 GHz, with a reflection coefficient of −47.3 dB.

To validate the proposed UWB antenna design, a prototype was fabricated, and the measured and simulated reflection coefficient (s_{11}) results are presented in Fig. (4). As shown in Fig. 4, the simulated and measured results exhibit close alignment, with, minor discrepancies attributed to fabrication tolerances, soldering losses, or other manufacturing imperfection or losses from soldering the SMA connector.

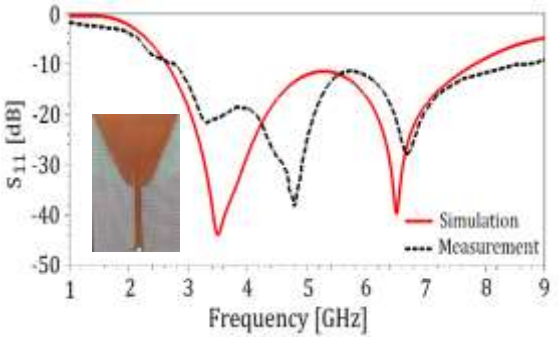

Figure (4): UWB antenna measured and simulated s_{11} parameter.

2.3. Design Low Pass Filter (LPF)

This section presents the design of a self-similar fractal-based LPF integrated into an ultra-wideband UWB antenna, forming a filtering antenna. The primary objective of this study is to suppress high-frequency signals detected by the transceiver system's antenna, as previously stated. To achieve this, an LPF is designed and incorporated into the feed line of the chamfered-edge UWB antenna. The LPF is engineered with a cutoff frequency of 3.5 GHz, targeting an improved signal-to-noise ratio (SNR) for the 3.5 GHz radio.

The proposed LPF structure, as depicted in Fig. (5), features an H-shaped fractal module designed to maximize element utilization within the filter's structure. The LPF is engineered with a cutoff frequency of 3.5 GHz, targeting an improved signal-to-noise ratio (SNR) for the 3.5 GHz radio. The filter is printed on the front side of an FR4 substrate with an overall dimensions ($W_s \times l_f$), a thickness of 0.8 mm, a relative permittivity of 4.3, and a loss tangent of 0.02.

The proposed LPF comprises a large rotated H-shaped strip geometry, representing the first-order fractal iteration, with dimensions ($l_l \times w_1$), centered on the substrate. A second-order fractal iteration includes two smaller H-shaped unit cells with dimensions ($l_2 \times w_2$), where $l_2 = l_1/5$ and $w_2 = w_1/10$. A pair of strip lines, comprising two sections with dimensions ($l_3 \times w_3$) and ($l_4 \times W_f$), are employed to ensure impedance matching to the 50 Ω ports connected to the filter. The optimized dimensions of the filter are summarized in Table (2).

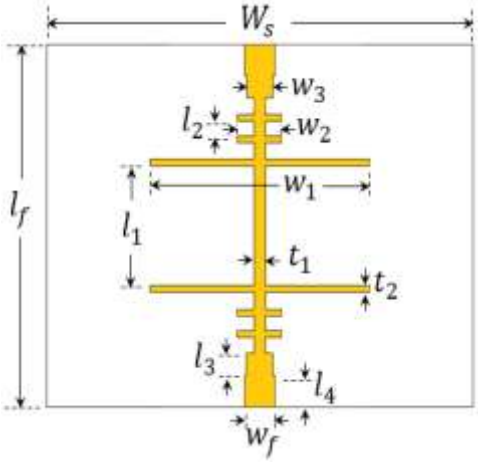

Figure (5): Geometry of the H-shaped fractal LPF

Table (2): Dimension details of the LPF.

Parameter Name	Value (mm)
W_s	29
W_f	2
w_1	15
w_2	3
w_3	1.8
l_f	16
l_1	5
l_2	0.5
l_3	1
l_4	1.4
t_1	0.8
t_2	0.4

The key parameter that influences the filter performance (reflection and transmission parameters, s_{11} and s_{21}, respectively) is the length of the large H-shaped strip branch w_1. Figs. (6a) and (6b) show the simulated s_{11} and s_{21} parameters (in dB), respectively, as a function of frequency (in GHz) for different- values of w_1 with values ranging from 13 mm to 17 mm and a step size of 1 mm. As Fig. (6a) shows, for an optimal w_1 of 15 mm (solid-red curve), the reflection coefficient remains below −35 dB around the target operating frequency of 3.5 GHz**,** Also, the frequency at which the minimum s_{11} occurs decreases as w_1 increases. On the other hand, as shown in Fig. (6b), frequency with minimum transmission parameter s_{21} (less than −45 dB) is decreased with increasing in w_1. Thus, the LPF design with inclusion of these fractal elements, successfully producing transmission zeros near the desired cutoff frequency of 3.5 GHz.

The fabricated LPF alongside its simulated and measured s_{11} and s_{21} results are plots in Fig. 7. It is demonstrating from Fig. (7) that the proposed LPF achieves a stopband attenuation exceeding -10 dB from 1 GHz to 3.5 GHz, with a transmission loss in the stopband reaching values below -40 dB. The -3 dB cut-off frequency is 3.5 GHz, and the insertion loss remains under -0.5 dB.

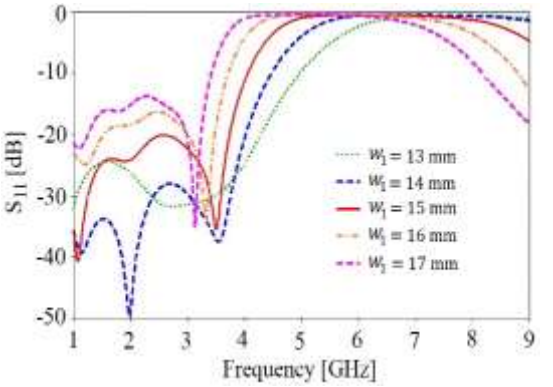

(a)

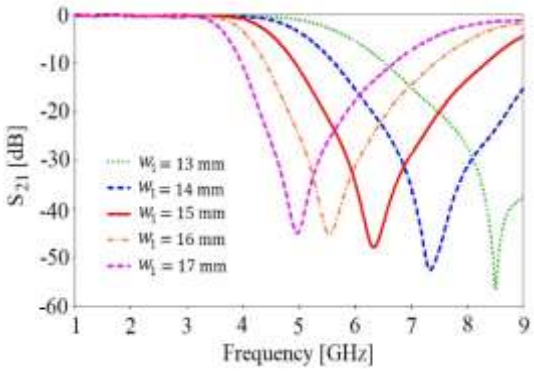

(b)

Figure (6): Characteristics of the filter**(a)** Reflection coefficient (s_{11}). **(b)** Transmission coefficient (s_{21}).

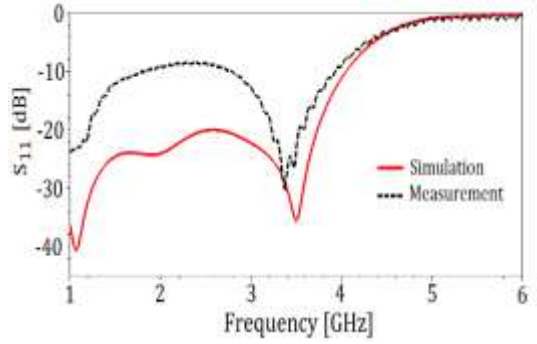

(a)

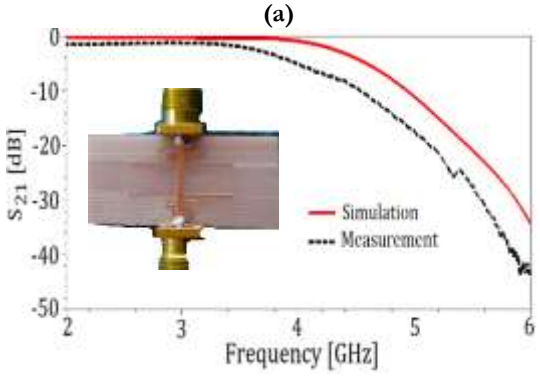

(b)

Figure(7): S-parameters characteristics of the LPF **(a)** s_{11} and **(b)** s_{21}.

2.3. UWB Filtering Antenna

The UWB filtering antenna is designed by integrating an H-unit cell filter into the feed line of the UWB antenna. Figure 8 illustrates the 3D structure of the antenna, showing both the front and back views. The antenna's total dimensions are 35 x 29 mm, and it is built on a 0.8 mm thick FR4 substrate with a dielectric constant of $\varepsilon_r = 4.3$ and a loss tangent of t = 0.02. The LPF attenuates high-frequency components, allowing only the low-frequency signals within its passband to reach the radiating patch. As a result, the excitation currents that fall within the LPF's passband are effectively delivered to the radiating patch, while high-frequency components are suppressed. This converts the chamfered-edge UWB antenna into a narrowband antenna that meets the 3.5 GHz communication requirements.

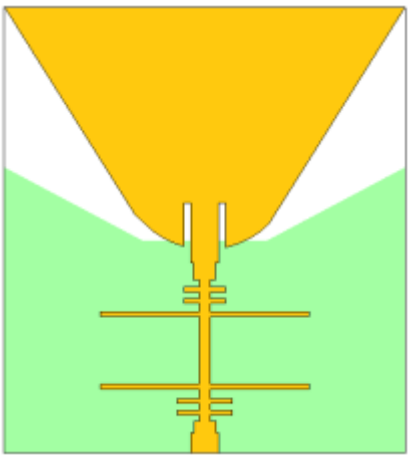

Figure (8): The proposed UWB filtering Antenna.

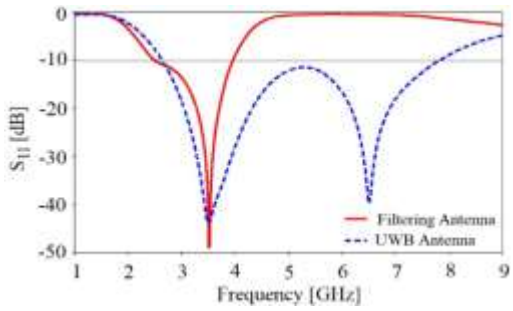

(a)

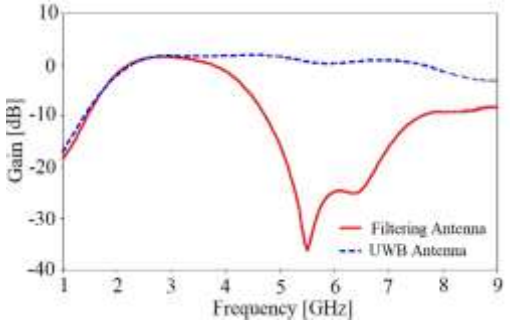

(b)

Figure (9): Filtering antenna S-parameter and gain**.** **(a)** Simulated s_{11}. **(b)** Simulated antenna gain.

The filtering antenna has a 43.7% impedance bandwidth and is centered at 3.5 GHz.The frequency responses for simulated filtering antennas with the aforementioned UWB antenna are illustrated in Figure

(9).Both the UWB and filtering antennas function at 3.5 GHz with a maximum s_{11} attenuation, as shown in Fig. (9a). The comparison between the gain of filtering antennas and UWB antennais shown in Fig. (9b). The filtenna has a gain of more than 1.7dBi between 2.7 GHz and 3.9 GHz, with two gain zeros at 1 GHz and 5.67 GHz.

Figure (10) illustrates the surface current distribution for the filtering antenna in its conduction and blocking states. In the conduction state, at a frequency of 3.5 GHz, the current flows from the feed to the microstrip patch radiator, as depicted in Figure (10a). In contrast, during the blocking state, the current at the port is absorbed by the LPF and does not reach the radiator's edge, resulting in reduced radiation efficiency. A weak current is observed flowing from the waveguide port to the primary radiating patch, as shown in Fig. (10b), which represents the surface current distribution at the sample frequency of 5.4GHz.

3. Manufacturing and evaluation.

The proposed filtering antenna was manufactured as shown in Fig. (11). The simulated and measured results for both of the UWB antenna and filtering antenna shown in Fig. (12) demonstrate a good agreement, with minor discrepancies attributed to fabrication tolerance errors, dielectric constant uncertainties, or losses incurred during the soldering of the SMA connector or copper waste resulting from etching the plate.

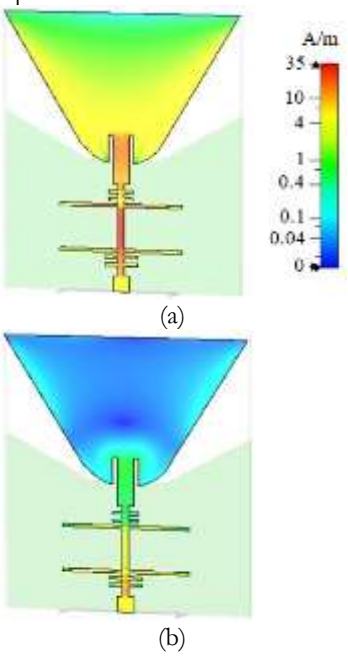

Figure (10): Current distribution surface. **(a)** operating condition at 3.5 GHz**. (b)** isolation state at 5.4 GHz.

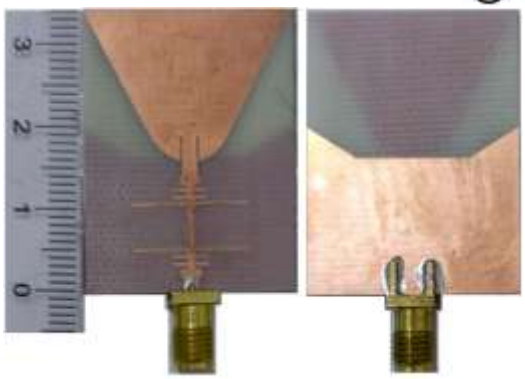

Figure (11): Manufactured filtering antenna. (a) Front side. (b) Back side.

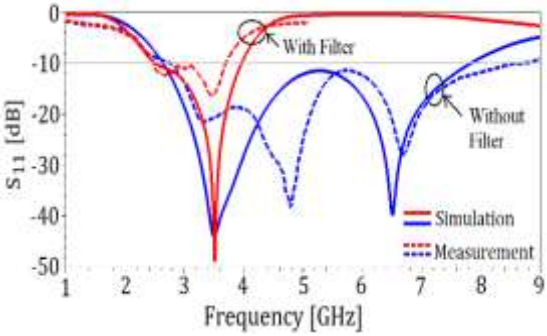

Figure (12): Measured and simulated s_{11} result for both UWB antenna and Filtering antenna

Figure (13a) depicts the simulated radiation pattern of the reference UWB antenna. The pattern exhibits omnidirectional characteristics with a horizontal figure-eight configuration along the elevation plane.

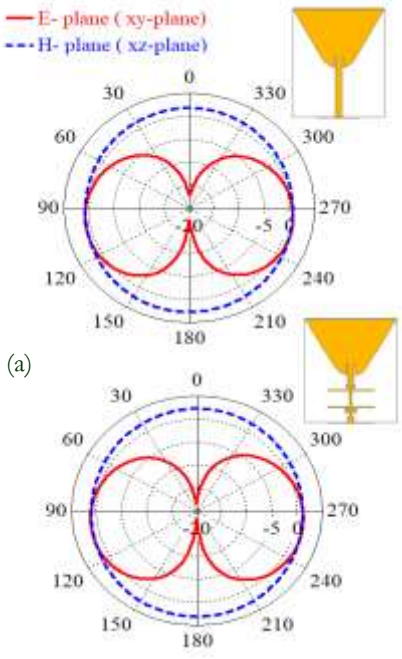

Figure (13): Radiation pattern at 3.5 GHz for (a) the reference UWB antenna. (b) filtering antenna proposed.

Table (3): Comparison with reported filtering antennas.

Ref.	Antenna Size in (mm)	Substrate (ε_r / h(mm))	BW (%)	Operating Frequency (GHz)	peak Gain (dBi)	Efficiency (%)	Extra Filtering structure	complexity
[2]	70 x 70	FR4 (4.2/0.508)	3	3.5-3.84	1.56	80	yes	Complex
[5]	43 x 30	FR4 (4.3/1.6)	29.5	2.1-2.82	2.96	75	yes	Simple
[10]	45 x 30	FR4 (4.3/1.6)	14	5.4-5.86	-1.3	NA	yes	Simple
[13]	66x80	FR4 (4.3/1.6)	13 22	4.7-5.1 5.4-6.2	2.6 3.7	NA NA	yes	Complex
[16]	47 x 29	FR4 (4.4/1.6)	25.7	5.4-6.7	1.6	NA	yes	Simple
[20]	24.5 x 20	FR4 (4.6/1.6)	27.6 20.9	3.24–4.2 9.12–10.25	2.33 2.8	86 73	yes	Complex
This work	**35 x 29**	**FR4 (4.3/0.8)**	**43.7**	**2.7-3.9**	**1.7**	**78**	**yes**	**Simple**

Conversely, Fig. (13b) illustrates the simulated radiation pattern of the filter-integrated antenna. The integration of the symmetrical filter structure enhances the symmetry of the radiation patterns in both the azimuth and elevation planes.

Table 3 provides a comparative analysis of the proposed filtering antenna against several recently reported filtering antennas. The results demonstrate that the proposed design is more compact and offers a larger percentage bandwidth compared to many of its counterparts. Furthermore, the peak gain and maximum radiation efficiency are sufficiently high to meet acceptable standards, making the prototypes well-suited for 3.5 GHz (WiMAX) application.

4. Conclusions

This paper describes a type of antenna that has a filter. The filter is low pass and its foundation is a center ramped obstruction line of transmission and a large fractal H-unit cell built inside the UWB antenna's microstrip feed line. It can be concluded that with this newly designed filter antenna, excellent filter, great suppression of harmonics up to 9 GHz and improved radiation characteristics were achieved. The antenna structure is customized for efficient operations across the UWB range with a fractional bandwidth of 102%. By adjusting the microstrip feed line, we change the UWB antenna so that it only resonates at a frequency of 3.5 GHz with bandwidth of approximately 43. 7% spanning from 2. 7 to 3. 9 GHz. Designing of LPF involved thorough parametric analysis to determine how dimensions of H-unit cell.

Accurate measurement of the lower cut off and transmission band widths is made feasible by the new H-unit cell. It is found that the constructed UWB filter-integrated antenna's measured and simulated properties are closely related. The recommended antenna runs at 78% radiation efficiency and has a gain of over 1.7 dBi. These results validate the efficiency of the proposed filtered antenna for communication system out-of-band suppression.

5. References

[1] C. A. Balanis, Antenna Theory: Analysis and Design, 4th ed., Wiley, 2016.

[2] A. Rezaul and T. Mohammad, "A compact filtering UWB antenna with enhanced band-notched characteristics," IEEE Trans. Antennas Propag., vol. 67, no. 3, pp. 1458-1467, 2019.

[3] Q. Meijun, L. Mingxing, L. Xiaoyan, and W. Wei, "A novel filtering antenna based on an embedded resonator for improved out-of-band rejection," Prog. Electromagn. Res. Lett., vol. 80, pp. 33-40, 2018.

[4] FCC, "First Report and Order 02-48," Federal Communications Commission, Washington, DC, USA, Apr. 2002.

[5] Z. Yingqi, Y. Wanchen, L. Xiaoyan, and W. Wei, "Wideband antenna with integrated filtering structure for out-of-band suppression," IEEE Antennas Wireless Propag. Lett., vol. 18, no. 4, pp. 785-789, 2020.

[6] X. Chen, F. Zhao, Y. Wanchen, and Z. Yingqi, "A compact filtering antenna with flat gain response within the passband," IEEE Antennas Propag., vol. 5, no. 12, 2019. https://doi.org/10.1109/LAWP.2013.2271972

[7] K. Gangwar, M. Alam, S. Kumar, and A. Kumar, "Filtering antennas: A technical review," Int. J. RF Microw. Comput.-Aided Eng., vol. 31, no. 10, e22797, 2021. https://doi.org/10.1002/mmce.22797

[8] C. Mao, Y. Zhang, Y. Wanchen, and Z. Yingqi, "Filtering antennas: Design methods and recent developments," IEEE Microw. Mag., vol. 22, no. 11, pp. 52-63, 2021. https://doi.org/10.1109/MMM.2021.3102199

[9] H. Mardani, C. Ghobadi, J. Nourinia, and M. Majidzadeh, "A simple compact monopole antenna with variable single- and double-filtering function for UWB applications," IEEE Antennas Wireless Propag. Lett., vol. 9, pp. 1076-1079, 2014. https://doi.org/10.1109/LAWP.2010.2091391

[10] J. Ren, Z. Xiong, Y. Wanchen, and Z. Yingqi, "A compact single-layer filtering patch antenna

with wide harmonic suppression and enhanced bandwidth," AEU-Int. J. Electron. Commun., vol. 145, p. 154083, 2022. https://doi.org/10.1016/j.aeue.2021.154083

[11] D. Tang, Y. Chen, Y. Wanchen, and Z. Yingqi, "Compact, wideband, planar filtenna with reconfigurable tripolarization diversity," IEEE Trans. Antennas Propag., vol. 67, no. 8, pp. 5689-5694, 2019. https://doi.org/10.1109/TAP.2019.2920298

[12] J. Deng, C. Tan, Y. Wanchen, and Z. Yingqi, "A compact dual-band filtering antenna for wireless local area network applications," Int. J. RF Microw. Comput.-Aided Eng., vol. 29, no. 9, e21822, 2019. https://doi.org/10.1002/mmce.21822

[13] M. Tang, Y. Chen, Y. Wanchen, and Z. Yingqi, "Experimentally validated, planar, wideband, electrically small, monopole filtennas based on capacitively loaded loop resonators," IEEE Trans. Antennas Propag., vol. 64, no. 8, pp. 3353-3360, 2016. https://doi.org/10.1109/TAP.2016.2560918

[14] P. Shome, T. Khan, S. Kumar, and A. Kumar, "Compact UWB-to-C band reconfigurable filtenna based on elliptical monopole antenna integrated with bandpass filter for cognitive radio systems," IET Microw. Antennas Propag., vol. 14, no. 10, pp. 1079-1088, 2020. https://doi.org/10.1049/iet-map.2019.0819

[15] A. Sahoo, D. Gupta, S. Kumar, and A. Kumar, "Highly selective integrated filter antenna for UWB application," Microw. Opt. Technol. Lett., vol. 59, no. 5, pp. 1032-1037, 2017. https://doi.org/10.1002/mop.30444

[16] B. Ramakrishnan and V. Sivashanmugham, "Chamfered edge filtering ultra-wideband antenna integrated with H-unit cell-loaded feed line for improved out-of-band rejection," Int. J. Microw. Wireless Technol., 2023. https://doi.org/10.1017/S1759078723000636

[17] D. Agrawal and J. Jadhav, "Filtering antennas: Synthesis and design," Int. Res. J. Eng. Technol. (IRJET), vol. 3, p. 6, 2016.

[18] Z. Ouadi, J. Amadid, M. Elhassouni, and A. El Bouzidi, "Compact microstrip filtenna designed for wireless local area network applications," in Proc. Int. Conf. Decision Aid Sci. Appl. (DASA), pp. 1593-1597, IEEE, 2022. https://doi.org/10.1109/DASA54658.2022.9765156

[19] Y. Yasir, M. K. Alkhafaji, A. H. Al-Khafaji, and H. A. Al-Raweshidy, "A new and compact wide-band microstrip filter-antenna design for 2.4 GHz ISM band and 4G applications," Electronics, vol. 9, no. 7, p. 1084, 2020. https://doi.org/10.3390/electronics9071084

[20] J. Jinn, S. Liao, Y. Wanchen, and Z. Yingqi, "Design of filtering-radiating patch antennas with tunable radiation nulls for high selectivity," IEEE Trans. Antennas Propag., vol. 66, no. 4, pp. 2125-2130, 2018. https://doi.org/10.1109/TAP.2018.2804661

[21] D. Chen, H. Zhang, Y. Wanchen, and Z. Yingqi, "A novel printed monopole antenna with stepped impedance hairpin resonator loading," IEEE Access, vol. 8, pp. 96975-96980, 2020. https://doi.org/10.1109/ACCESS.2020.2996623

[22] W. Wang, N. Ran, Y. Wanchen, and Z. Yingqi, "A novel differential filtering patch antenna with high selectivity," Int. J. RF Microw. Comput.-Aided Eng., vol. 29, no. 10, e21880, 2019. https://doi.org/10.1002/mmce.21880